Nuclear Physics A435 (1985) 844–858

SUB-SATURATION PHASES OF NUCLEAR MATTER

R.D. WILLIAMS and S.E. KOONIN

W. K. Kellogg Radiation Laboratory, California Institute of Technology, Pasadena, California 91125, USA

Received 27 July, 1984
(Revised 21 August 1984)

Abstract. We study the zero-temperature equation of state of isospin-symmetric nuclear matter below saturation density by minimizing the energy of the nucleons in a periodic cubic cell at each mean density. We take the energy per nucleon to be the Thomas–Fermi approximation to the Skyrme III functional and include the Coulomb energy. We find several phase transitions between different topologies of matter, going from spheres to rods to slabs to tubes to bubbles with increasing density, and discuss their implications for models of supernova core collapse.

1. Introduction

Uniform nuclear matter is unstable at a density somewhat below saturation; i.e. when the density derivative of the pressure becomes negative [1]). This occurs at a density of about 0.095 nucleons fm^{-3} ($1.6\times10^{14}\,g\,cm^{-3}$), which is 65% of the saturation density. The thermodynamically favored configuration (of lower free energy) is then a mixture of saturated matter and vacuum, in much the same way that the homogeneity of a fluid is disrupted when its density is intermediate between that of the liquid and gas phases. In this paper, we investigate the structure of this mixture, assuming a uniform admixture of electrons for overall electrical neutrality. The structure is determined by competition between the short-range surface force and the long-range Coulomb force: the surface energy is reduced with aggregation (because the ratio of surface area to volume is reduced) while the Coulomb energy is reduced by dispersion of the matter (due to the inter-proton repulsion). The equation of state of matter in this density regime thus depends on the equilibrium configuration of the interface between the nuclear matter and the vacuum.

In addition to its intrinsic interest, this sub-saturation density regime exists briefly in a collapsing stellar core during the formation of a type II supernova [2-5]), and the strength – or even existence – of the subsequent shock wave depends sensitively upon the equation of state. Just before collapse, the central iron core is supported against gravity by the pressure of the electron gas, and, when collapse starts, the central density increases. This causes the protons to capture electrons, further reducing the available electron pressure, and so creating a positive feedback which drives the catastrophic collapse. It is the stiffness of the nuclear equation of state at saturation density which halts the collapse and causes a bounce of the core. The

rebounding core meets the infalling outer layers of the star, forming a shock and expelling material to create an expanding nebula. The formation of a strong shock is aided by the homologous property of the collapsing core (i.e. the inward velocity of the matter being proportional to its radius). Any phase transition of the collapsing matter will absorb heat, disrupt the homology, and so weaken the subsequent shock. Although the latent heat associated with such transitions might be small, the shock formation is delicate enough that they may be relevant and therefore it is possible that other physical mechanisms will be required to explain the observed properties of supernovae [6]). For densities below about 35% of saturation, the nuclear pressure is much smaller than the electron pressure, while above about 75% of saturation the nuclear equation of state is that of uniform matter. However, between these two limits it is essential to determine the equation of state as accurately as is possible.

To date, calculations of nuclear matter in this regime have assumed either spherical nuclei, spherical bubbles immersed in uniform nuclear matter, or uniform matter, and have been done using the compressible liquid drop model [7,8]), or the Hartree–Fock method [9,10]), or the extensive treatment of Lamb, Lattimer, Pethick and Ravenhall [11]). However, it has been shown by Ravenhall, Pethick and Wilson [12]) that, with increasing density, there are other transitions - from spherical nuclei to a rod-like geometry, to slabs, to tubes (cylindrical bubbles), to spherical bubbles, and then to uniform matter. Their calculation was at zero temperature, with equal numbers of protons and neutrons, and used a simple surface energy for the interface separating the uniform saturated nuclear matter from vacuum. The total energy is then minimized with respect to central density and nuclear size for fixed mean density. The surface shape was modeled in the Wigner–Seitz approximation, so that a spherical nucleus was surrounded by a spherical surface of zero electrostatic potential and a cylindrical nucleus by a cylindrical zero equipotential. There was thus only one independent coordinate in 1, 2, or 3 dimensions, and the surface shape was *a priori* limited to one of the six possibilities above. Ravenhall *et al.* therefore could not examine the stability of these shapes under symmetry breaking or the nature of the transitions between them, and the set of possible surfaces was restricted to those with a convenient accompanying coordinate system. Ravenhall *et al.* interpolated between these shapes by using a non-integral dimensionality for the Wigner–Seitz cell, minimizing with respect to this dimensionality; unfortunately physical relevance of this interpolation is not explained.

In this paper we improve on the calculation of Ravenhall *et al.* by allowing the nuclear matter to assume an arbitrary configuration within the unit cell. We describe the matter by considering the local number density of nucleons at each site of a periodic cubic lattice filling the unit cell; the free energy (or equivalently, at zero temperature, the thermodynamic potential) is then reduced by a relaxation process until a local minimum is achieved. The lattice is fine enough to reproduce the nuclear surface accurately and the system is free to adopt its lowest energy within the constraint of cubic periodicity. For this exploratory study we have worked in the

zero-temperature limit and have taken the proton and neutron densities to be equal. [This last assumption means that there is no neutron gas surrounding the nuclei [13].] The use of a cubic unit cell is purely for computational convenience, and other geometries such as face- or body-centered cubic would be equally valid. Relaxation of all these assumptions is straightforward, although at the expense of increased computation.

2. Description of the model

2.1. THE ENERGY FUNCTIONAL

We can safely assume that the electrons decouple from the nuclear matter, except in the sense of providing overall charge neutrality. This is so because, for the densities of interest, the Fermi energy of the electron gas is much larger than variations in the Coulomb potential across the unit cell. In the usual linearization of the Thomas-Fermi description the electron screening length is given by

$$\left[\frac{\hbar^2(96\pi^2\langle\rho\rangle)^{-1/3}}{me^2}\right]^{1/2} \approx 150\ \text{fm}\,, \tag{1}$$

where m is the electron mass, and $\langle\rho\rangle$ is the mean density. Since this is much larger than any of the nuclear length scales involved, the electron gas provides an essentially uniform background of negative charge.

Our calculations consider all possible density configurations which have periodic cubic symmetry throughout all of space. We take the energy functional to be the Skyrme functional [14] in the zero temperature Thomas-Fermi approximation [15] plus the Coulomb energy, simplifying to equal proton and neutron densities. The internal energy density U is then the sum of bulk (E_B), surface (E_S) and Coulomb (E_C) energy densities; the bulk and surface energies are those of the Skyrme interaction, and, as we neglect the Coulomb exchange energy [15], the Coulomb energy is just the classical expression. The thermodynamic potential per unit volume at zero temperature is then

$$\begin{aligned}\Omega &= U-\mu\langle\rho\rangle = E_B+E_S+E_C-\mu\langle\rho\rangle \\ &= L^{-3}\int \rho(r)[e(\rho(r))-\mu]+\alpha_S|\nabla\rho(r)|^2+\tfrac{1}{2}V(r)\tfrac{1}{2}\rho(r)\,\mathrm{d}^3r\,,\end{aligned} \tag{2}$$

where μ is the chemical potential, and $\langle\cdots\rangle$ denotes a spatial average. The integral is over the volume of the cubic cell of side L, and the Coulomb energy expression uses the proton density $\rho_p=\frac{1}{2}\rho$ and the electrostatic potential

$$V(r)=\tfrac{1}{2}e^2\int\frac{\rho(r')-\langle\rho\rangle}{|r-r'|}\,\mathrm{d}^3r'\,. \tag{3}$$

The $\langle\rho\rangle$ term above comes from the uniform electron charge density, and note that

the integral (3) is over all space, not just a single unit cell. The energy per nucleon is the Thomas–Fermi approximation to the Skyrme III functional,

$$e(\rho)=\tfrac{3}{8}t_0\rho+\tfrac{1}{16}t_3\rho^2+\tfrac{3}{5}(\tfrac{3}{2}\pi^2)^{2/3}\rho^{5/3}\left[\tfrac{1}{16}(3t_1+5t_2)\rho+\frac{\hbar^2}{2M}\right], \tag{4}$$

with $t_0=-1128.75\ \text{MeV}\cdot\text{fm}^3$, $t_1=395.0\ \text{MeV}\cdot\text{fm}^5$, $t_2=-95.0\ \text{MeV}\cdot\text{fm}^5$, $t_3=14000\ \text{MeV}\cdot\text{fm}^6$, $\hbar^2/M=41.47\ \text{MeV}\cdot\text{fm}^2$, and we have used the zero-temperature Thomas–Fermi expression for the kinetic energy density. Finally, the coefficient of the $|\nabla\rho|^2$ term is

$$\alpha_S=\tfrac{1}{64}(9t_1-5t_2)=62.97\ \text{MeV}\cdot\text{fm}^5. \tag{5}$$

An equilibrium state of the system is one which minimizes the thermodynamic potential functional with respect to the density function. The change in Ω for a change in the density $\delta\rho(r)$ is

$$\delta\Omega=L^{-3}\int[\varepsilon'(\rho)-\mu-2\alpha_S\nabla^2\rho+\tfrac{1}{2}V(r)]\delta\rho(r)\,\mathrm{d}^3r. \tag{6}$$

where we have introduced $\varepsilon(\rho)=\rho e(\rho)$, and $\varepsilon'(\rho)=\mathrm{d}\varepsilon/\mathrm{d}\rho$. For a fixed μ, there may of course be several equilibrium configurations. All of them satisfy

$$2\alpha_S\nabla^2\rho-\tfrac{1}{2}V(r)-\varepsilon'(\rho)+\mu=0. \tag{7}$$

We have not as yet defined E_B, E_S, and E_C, but only their sum. The Coulomb energy is the third term in the integrand of (2), and E_B, E_S can be obtained as follows. Consider a plane interface between saturated matter, with nucleon number density ρ_s, with no Coulomb interaction, and with the z-axis normal to the interface. Then (7) can be integrated,

$$\alpha_S\left(\frac{\mathrm{d}\rho}{\mathrm{d}z}\right)^2=\varepsilon(\rho)-\mu\rho+K, \tag{8}$$

where K is an integration constant. For $z\ll 0$ or $z\gg 0$, $\rho\to\rho_s$ or $\rho\to 0$, so

$$\begin{aligned}\alpha_S\left(\frac{\mathrm{d}\rho}{\mathrm{d}z}\right)^2&=\varepsilon(\rho)-\frac{\rho}{\rho_s}\varepsilon(\rho_s)\\ &\to\int\varepsilon(\rho)-\alpha_S\left(\frac{\mathrm{d}\rho}{\mathrm{d}z}\right)^2\mathrm{d}z=\frac{\varepsilon(\rho_s)}{\rho_s}\int\rho\,\mathrm{d}z.\end{aligned} \tag{9}$$

The right side is the bulk energy E_B, since it is the energy per nucleon at saturation times the number of nucleons. We conclude that

$$\begin{aligned}E_B&=\int\varepsilon(\rho)-\alpha_S|\nabla\rho|^2\,\mathrm{d}^3r,\\ E_S&=\int 2\alpha_S|\nabla\rho|^2\,\mathrm{d}^3r.\end{aligned} \tag{10}$$

2.2. ANALYTIC ESTIMATES

We expect that solutions of (7) are characterized by regions of saturation density and vacuum, separated by an interface whose area is proportional to the surface energy. An analytic estimate can be obtained, following Ravenhall, Pethick and Wilson [12]), by finding the lowest energy of a set of simple shapes within the cubic cell with periodic boundary conditions. We take this set to be the sphere, rod, slab, tubular bubble, and spherical bubble, and the density to be either zero or saturation density, $\rho_s = 0.145\,\mathrm{fm}^{-3}$. Let $u = \langle\rho\rangle/\rho_s$ be the fraction of the unit cell filled with saturated nuclear matter, $e(\rho_s)$ the energy per nucleon of saturated matter, and d the "dimensionality" of the phase ($d = 3$ for spheres, $d = 2$ for rods, and $d = 1$ for slabs). The surface energy density is then $E_S = u\sigma d/R$, where σ is the surface energy and R the radius of the shape (defined below). The bulk energy density is $E_B = u\rho_s e(\rho_s)$ and the Coulomb energy density is

$$E_C = \tfrac{1}{2}\pi\langle\rho\rangle^2 e^2 R^2 u f_d(u)\,, \tag{11}$$

where, for spheres,

$$u = \frac{4\pi R^3}{3L^3}\,, \qquad f_3(u) = \frac{3L}{4\pi^3 R}\sum_{\kappa\in Z^3,\kappa\neq 0}\frac{j_1^2(2\pi|\kappa|R/L)}{\kappa^4}\,, \tag{12}$$

for rods,

$$u = \frac{\pi R^2}{L^2}\,, \qquad f_2(u) = \frac{L^2}{4\pi^3 R^2}\sum_{\kappa\in Z^2,\kappa\neq 0}\frac{J_1^2(2\pi|\kappa|R/L)}{\kappa^4}\,, \tag{13}$$

and for slabs,

$$u = R/L\,, \qquad f_1(u) = (1-u)^2/3u\,. \tag{14}$$

Here, J_1, j_1 are regular cylindrical and spherical Bessel functions, respectively, and the sums in (12) and (13) are over all non-zero triples or pairs of integers, respectively. Similar expressions can be derived for the bubble and tube configurations. We then minimize U with respect to R, and take the phase with the lowest U to obtain the thermodynamically favored configuration for a given $\langle\rho\rangle$. This minimization can be done immediately since the surface energy is proportional to R^{-1}, and the Coulomb energy density is proportional to R^2. Thus $R^3 = \sigma d/\pi\langle\rho\rangle^2 e^2 f_d(u)$, L is determined from R and u, and $E_S = 2E_C$. The chemical potential μ is then $\mathrm{d}U/\mathrm{d}\langle\rho\rangle$, and the nuclear pressure is $\mu\langle\rho\rangle - U$. In our calculations we adopt $\sigma = 1.096\,\mathrm{MeV}\cdot\mathrm{fm}^{-2}$, the value associated with the Skyrme interaction we use [16]).

2.3. DISCRETIZATION AND RELAXATION

We now consider the numerical solution of the non-linear integral-differential equation (7). We divide the periodic cubic cell of size L into N^3 small cubic cells

labelled by the integer vector $i \in Z^3$. The finite-difference expressions for the energy densities in terms of the number density ρ_i at i are then

$$E_B + \tfrac{1}{2}E_S = N^{-3}\sum_i \varepsilon(\rho_i)\,, \tag{15}$$

$$\tfrac{1}{2}E_S = \alpha_S N^{-1}L^{-2}\sum_i (\rho_i - \rho_{i'})^2\,, \tag{16}$$

$$E_C = \tfrac{1}{2}e^2 N^{-4}L^2 \sum_i \sum_j \tfrac{1}{2}(\rho_i - \langle\rho\rangle)\tfrac{1}{2}(\rho_j - \langle\rho\rangle)|i-j|^{-1}\,, \tag{17}$$

where i' represents a nearest-neighbor of i, and i, j are integer vectors, i ranging over the N^3 lattice points, j unrestricted. Minimizing the energy with respect to L at equilibrium shows immediately the virial theorem $E_S = 2E_C$, since the exponents of L in (16) and (17) are equal and of opposite signs. This result is in agreement with the analytic model above and ref. [12]). The pressure is the sum of the electron pressure $\frac{1}{8}(\frac{3}{2}\pi^2)^{1/3}\hbar c\langle\rho\rangle^{4/3}$ and the nuclear pressure $\mu\langle\rho\rangle - U$.

The equation to be solved is then the finite-difference analogue of (7),

$$-\frac{N^3h^2}{12\alpha_S}\frac{\partial\Omega}{\partial\rho_i} \doteq 0 = Q_i - \rho_i - S(\rho_i)\,, \tag{18a}$$

where

$$Q_i \equiv a_i - \frac{h^2}{12\alpha_S}[\tfrac{1}{2}V_i - \mu]\,, \tag{18b}$$

$$S(\rho) \equiv \frac{h^2\varepsilon'(\rho)}{12\alpha_S}\,. \tag{18c}$$

Here, a_i is the average density of the six nearest neighbors of i, V_i is the Coulomb potential at i, and $h = L/N$ is the lattice spacing.

To solve (18) iteratively, we could make an initial guess for the solution and then use successive relaxation, in which the change in ρ_i is proportional to the right side of (18a), so that the change in Ω is negative definite and the system moves toward a local minimum. [This process is also called the imaginary time step method [17]).] The relaxation step would then be to set ρ_i equal to the average of its neighbors, a_i, with corrections of order h^2; i.e. the Gauss–Seidel method of relaxation. However, there are two problems in applying this method to the present problem. First, it is possible for the density at a point to be unphysically negative, requiring that an artificial cutoff be imposed at zero density. More importantly, it assumes that h is small compared to the nuclear surface thickness. When h is comparable to this thickness, as we would like for computational efficiency, then $S(\rho_i)$ is comparable to ρ_i and it is better to solve (18a) for ρ_i directly. This can be accomplished with a table lookup: for a given Q there is a single solution ρ of the equation $\rho + S(\rho) = Q$. Notice that Q_i is only weakly dependent on ρ_i. Thus we no longer have to assume that $Q_i - S(\rho_i)$ is weakly dependent on ρ_i, which is true only for small h. The problem of negative density is also eliminated, since the solution table $\rho(Q)$ is

smooth and never negative. Thus our relaxation step is to cycle through the lattice and solve (18a) at each site, replacing ρ_i by the solution. The fact that (18a) should have a unique solution places a limit on the lattice spacing. We need the right side of (18) to be monotonic in ρ, so that its derivative must be greater than zero (for a unique solution), implying $h^2 < -12\alpha_S/\min \varepsilon''(\rho)$, or $h \lesssim 1.4$ fm. This is an upper limit, and we found that $h \lesssim 1$ fm was the largest reasonable value we could use.

We found that, just as with the Gauss-Seidel method, our direct solution method was greatly improved by over-relaxation [18]). It is well known that the Gauss-Seidel method can be made an order of magnitude more efficient by over-relaxation: instead of the step $\rho \to \rho_{\text{new}}$, use $\rho \to \omega\rho_{\text{new}} + (1-\omega)\rho_{\text{old}}$, where ω is unity for Gauss-Seidel, and optimally between 1 and 2. We found empirically that a value of ω between 1.55 and 1.6 was optimal.

For the interesting (non-uniform) solutions of (7), the thermodynamic potential is a minimum with respect to each ρ_i for constant $\langle\rho\rangle$, but a maximum with respect to $\langle\rho\rangle$. Thus, the only energy minima are the uninteresting ones consisting of uniform saturated matter and uniform vacuum. To demonstrate this we take the space average of the stationarity equation (7) to obtain $\mu = \langle\varepsilon'(\rho)\rangle$. Elementary thermodynamic relations imply that

$$\frac{\partial^2\Omega}{\partial\langle\rho\rangle^2} = \frac{\partial\mu}{\partial\langle\rho\rangle} = \frac{\partial\langle\varepsilon'\rangle}{\partial\langle\rho\rangle}. \tag{19}$$

Since $\varepsilon'(\rho)$ is monotonically decreasing in the intermediate density range, $\partial^2\Omega/\partial\langle\rho\rangle^2 < 0$, demonstrating instability. We therefore use a more "active", quadratic constraint and consider the functional

$$\Omega' = U + \lambda\langle\rho\rangle(\langle\rho\rangle - \bar{\rho}), \tag{20}$$

with λ and $\bar{\rho}$ to be chosen. The stationarity condition for Ω' is then modified to

$$2\alpha_S\nabla^2\rho - \tfrac{1}{2}V(r) - \varepsilon'(\rho) - \lambda(2\langle\rho\rangle - \bar{\rho}) = 0. \tag{21}$$

When the relaxation has converged and (21) is satisfied, the chemical potential is given by $\mu = -\lambda(2\langle\rho\rangle - \bar{\rho})$. With this constraint the modified thermodynamic potential Ω' is now a minimum with respect to *any* variation of the density field, as long as $2\lambda > \partial\mu/\partial\langle\rho\rangle$; if λ becomes too large, though, the numerical method develops an odd-even instability. We used $\lambda = 300\ \text{MeV}\cdot\text{fm}^{-3}$ for most of the calculations, except in the cases of the smallest spheres and the smallest bubbles, when a much stronger constraint (large λ) is necessary to keep the system from uninteresting uniformity.

The above arguments can be applied straightforwardly for a higher-order approximation to the second derivative of ρ, so that ∇^2 is a five-point instead of a three-point finite-difference expression:

$$\frac{\mathrm{d}^2\rho}{\mathrm{d}x^2} \approx [-\rho_2 + 16\rho_1 - 30\rho_0 + 16\rho_{-1} - \rho_{-2}]/(12h^2), \tag{22}$$

with the obvious notation. The only difference in the relaxation is that the average a_i is now a weighted mean of 12 neighboring points, and the expression $12\alpha_S$ in (18) becomes $15\alpha_S$. We used the five-point expression for the calculations, both for the stationarity condition (7) and for the Coulomb potential, and also in the calculation of the surface energy.

One might hope to avoid the exact calculation of the Coulomb potential at each step by simultaneously relaxing the Poisson equation with the density. However the natural rates for these two relaxations are very different because of disparate strengths of the nuclear and Coulomb forces; one would have to relax the Coulomb potential ~35 times as often as the density. It is therefore better to use fast Fourier transform methods to evaluate the Coulomb potential exactly before each density relaxation. The computation is then most efficient if the lattice size N is a power of two, and we used a 32^3 lattice for our computations. With a maximum allowable spacing of ~1 fm, the maximum cell size is then ~32 fm.

One vital check of the relaxation algorithm is that the thermodynamic potential decrease monotonically, which it did in our single precision calculation to five significant figures. We also checked the evaluation of the Coulomb energy by comparing it with the analytic results for sharp-surface configurations (12)-(14), and found equality to within discretization error. A further check was that the surface energy of converged spherical configurations agree with that derived from the surface tension of the Skyrme functional. We also checked that the internal energy is indeed minimized with respect to L when $E_S = 2E_C$, and thereafter used the ratio E_S/E_C to adjust L until the ratio was 2. Thus, the convergence process was as follows: relax with fixed L until the chemical potential has been constant (within 10^{-5}) for 30 iterations, and then, if $E_S/2E_C$ is not unity (to within 10^{-4}), multiply L by $(E_S/2E_C)^{0.23}$, and relax again (the value 0.23 was empirically determined). We started the relaxation either with a lattice of uncorrelated random densities, uniformly distributed between zero and saturation density or in a smooth surface (thickness $\approx$ 1 fm) realization of one of the phases (sphere, rod, slab, tube, bubble) discussed in the model of subsect. 2.2.

The computational effort required is quite substantial due to the different magnitudes of the nuclear force (which creates the surface) and the Coulomb force (which arranges the nuclear matter globally). Within ten or so iterations a random start polarized into regions of vacuum or saturation density, but it took several hundred iterations for the chemical potential to stabilize. On a VAX 11/750 with floating-point accelerator the 32^3 lattice took about 40 s of CPU time per iteration.

3. Results and discussion

In fig. 1 we show the quantity $\bar{U} = U + 11\langle\rho\rangle + 35\langle\rho\rangle^2$ as a function of $\langle\rho\rangle$, where $\langle\rho\rangle$ is in fm^{-3} and U in MeV · fm^{-3}. We plot $\bar{U}$ instead of U because the energy differences between the phases are quite small compared to the total internal energy.

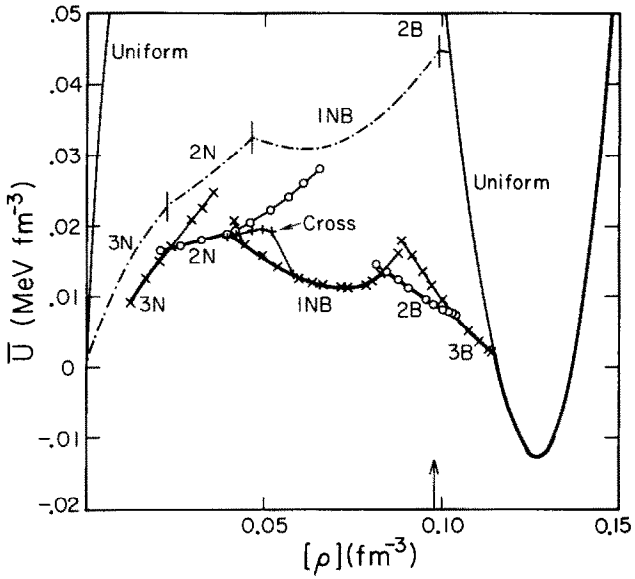

Fig. 1. The adjusted internal energy $\bar{U}$ of nuclear matter, as a function of the mean density $\langle\rho\rangle$. Plotted symbols show the results of individual calculations, connected by a solid line. The thermodynamically favored phase is shown by a heavy line and the results of the analytic model by a chained line.

In this and subsequent figures we use the notation of ref. [12]): 3N for three-dimensional nuclei (spheres), 2N for two-dimensional nuclei (rods), 1NB for alternating slabs of matter and vacuum, 2B for two-dimensional bubbles (tubes), and 3B for three-dimensional bubbles. We have also found a phase "cross", an intermediate between 2N and 1NB, which is the slab configuration with regular holes, like a stack of wire mesh. By increasing the mean density adiabatically, the cross phase changes to the 1NB phase, so that its energy coincides with that curve. This cross phase has minimum energy for a small range of $\langle\rho\rangle$ near 0.04 fm^{-3}, but would be washed out easily by a finite temperature. The thermodynamically favored phase, with the minimum $\bar{U}$, is shown with a heavy line.

Also shown in fig. 1 are the corresponding results from the model subsect. 2.2, shown with a chained line; the internal energy is greater for the model because the variational space is considerably more restricted and because it treats the surface poorly. The analytic model has no 3B phase and barely has a 2B phase. This is because the model assumes that the nuclear matter density can be only one fixed value, saturation density, and a better treatment, minimizing also with respect to the nuclear matter density, would demonstrate these phases too, as in ref. [12]). The density at which $dP/d\langle\rho\rangle = 0$ for the uniform phase, at $\langle\rho\rangle = 0.9745$ fm^{-3}, is shown with a vertical arrow. Above this density, uniform matter is metastable. That is, it is stable with respect to small perturbations, but is unstable with respect to finite perturbations until the density exceeds 0.1151 fm^{-3}, when the 3B phase ends.

TABLE 1

Phase transitions of nuclear matter in the sub-saturation regime, with critical density, pressure and chemical potential discontinuities, and the pressure of the mixture by Maxwell construction (the results of the analytic model of subsect. 2.2 are shown in parentheses)

Phase transition	ρ [fm^{-3}]	ΔP [MeV · fm^{-3}]	$\Delta\mu$ [MeV]	P_{mix} [MeV · fm^{-3}]
3N-2N	0.0229	−0.003	−0.1	0.39
(3N-2N)	(0.0224)	(−0.006)	(−0.3)	
2N-1NB	0.0423	+0.033	+0.8	
(2N-1NB)	(0.0465)	(−0.032)	(−0.7)	
1NB-2B	0.0842	−0.16	−2.1	2.05
(1NB-2B)	(0.0990)	(−0.07)	(−0.7)	
2B-3B	0.1026	−0.12	−1.5	2.60
3B-U	0.1151	−0.37	−3.5	2.89
(2B-U)	(0.1023)	(−0.42)	(−4.1)	

Since $dU/d\langle\rho\rangle$ is discontinuous, there are first-order transitions between the phases. Table 1 shows the densities at which the phase-transitions occur, together with the pressure discontinuity and the discontinuity of μ. Also shown in parentheses is the same information for the model of subsect. 2.2. Of course, the phase transitions are not physical discontinuities of the pressure. On the line connecting two phases, the physical system is a mixture of the two phases, and the functional form of this connecting line is obtained from a Maxwell construction [19]), so that the total pressure is constant for the mixture. Thus $P + P_e = P_{mix}$, where P_{mix} is a constant from the construction, and P_e is the electron pressure. The fifth column of table 1 shows P_{mix} for all the phase transitions except 2N-1NB, in which the pressure change is positive and the Maxwell construction does not apply.

Fig. 2 shows the cell size L which minimizes the internal energy. There is qualitative agreement with the analytic model, shown by a chained line. The cell size for the cross configuration is also shown; at higher density it changes to the 1NB configuration, but with the slabs tilted diagonally, so that the cell size is greater by a factor of $\sqrt{2}$.

Fig. 3 shows our results for the chemical potential. There is qualitative agreement with the analytic model, shown with a chained line, but the discontinuities are greater. Fig. 4 shows the nuclear specific pressure, $P/\langle\rho\rangle$: the results of the model calculation (chained), and the specific pressure for the uniform phase; the heavy line is the thermodynamically favored pressure. Figs. 3 and 4 contain some numerical fluctuations because the quantities plotted are differences between much larger numbers and because there is no unambiguous convergence criterion for the relaxation process. The adiabatic change from the cross phase to the 1NB phase is shown,

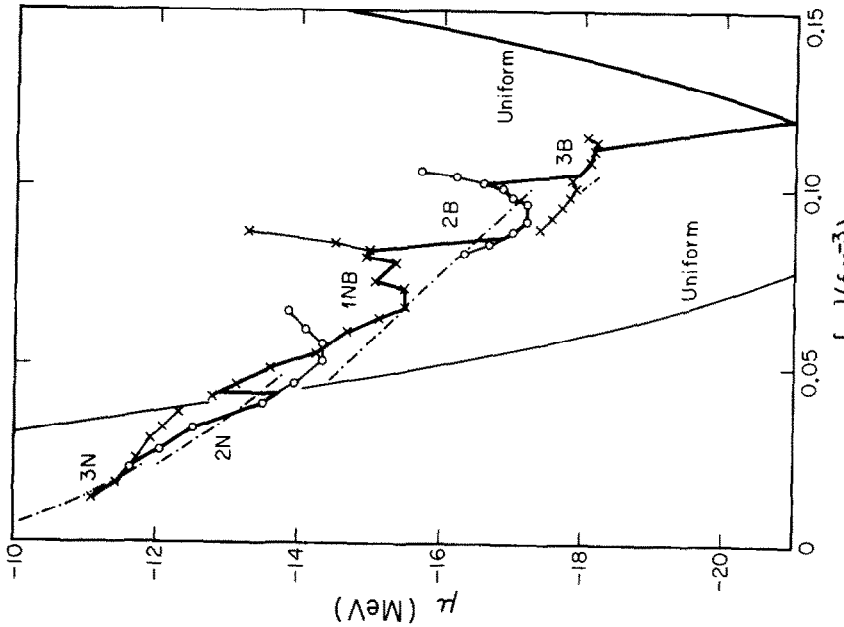

Fig. 3. The chemical potential μ as a function of $\langle\rho\rangle$. The notation is as in fig. 1.

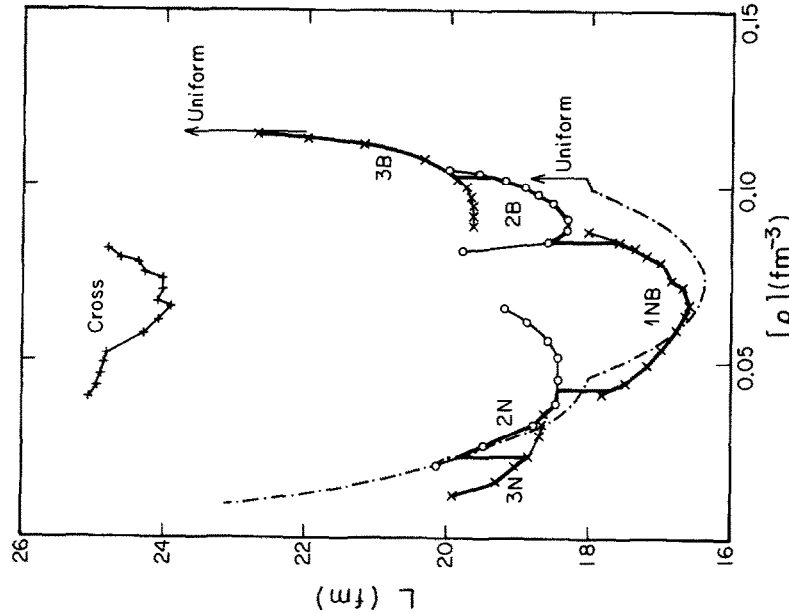

Fig. 2. The cubic cell size L as a function of $\langle\rho\rangle$. The notation is as in fig. 1.

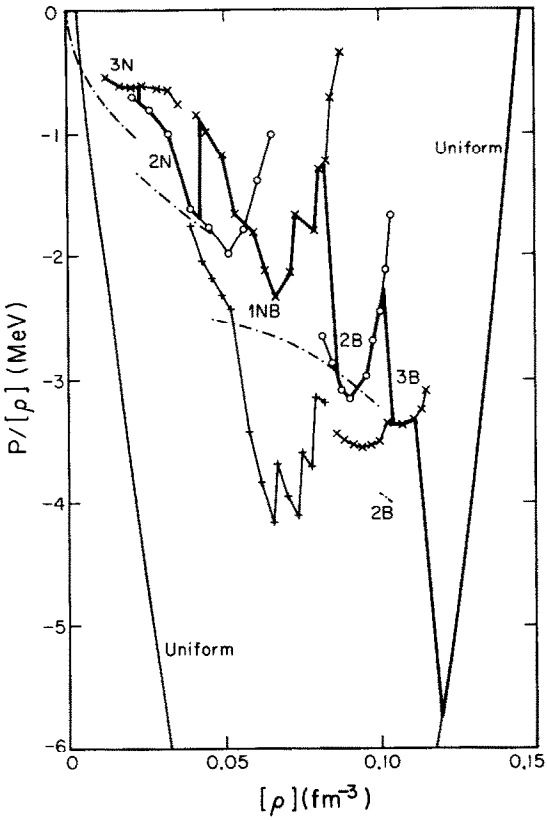

Fig. 4. The nuclear specific pressure $P/\langle\rho\rangle$ as a function of $\langle\rho\rangle$. The notation is as in fig. 1.

with the very negative pressures at around 0.07 fm^{-3} caused by the system being in a "wrong" (metastable) phase.

Fig. 5 shows the distribution of nuclear matter within the periodic unit cell for four mean densities. Each set of eight panels corresponds to one density value, and each of the eight panels is a contour plot of the local nuclear density. The two coordinates of each contour plot vary from 0 to L. The third coordinate is constant for each panel and assumes eight equally spaced values from 0 to L for each of the eight panels. The shaded regions of the plots have $\rho > 0.1$ fm^{-3}. The first density value, 0.039 fm^{-3}, is in the cross phase, the next two are intermediate densities in the adiabatic change to the fourth plot, which is the diagonally slanted 1NB phase, at mean density 0.082 fm^{-3}. For the panel at density 0.058 fm^{-3}, the system is exactly balanced between the two phases, as can be seen by the double-valued density of the nuclear matter, which is why the pressure is so negative ($P/\rho \approx -3.4$ MeV · fm^3) for that configuration.

The data in the first panel of fig. 5 result from relaxing an initial lattice of random densities; the other panels were obtained from the relaxed configuration by

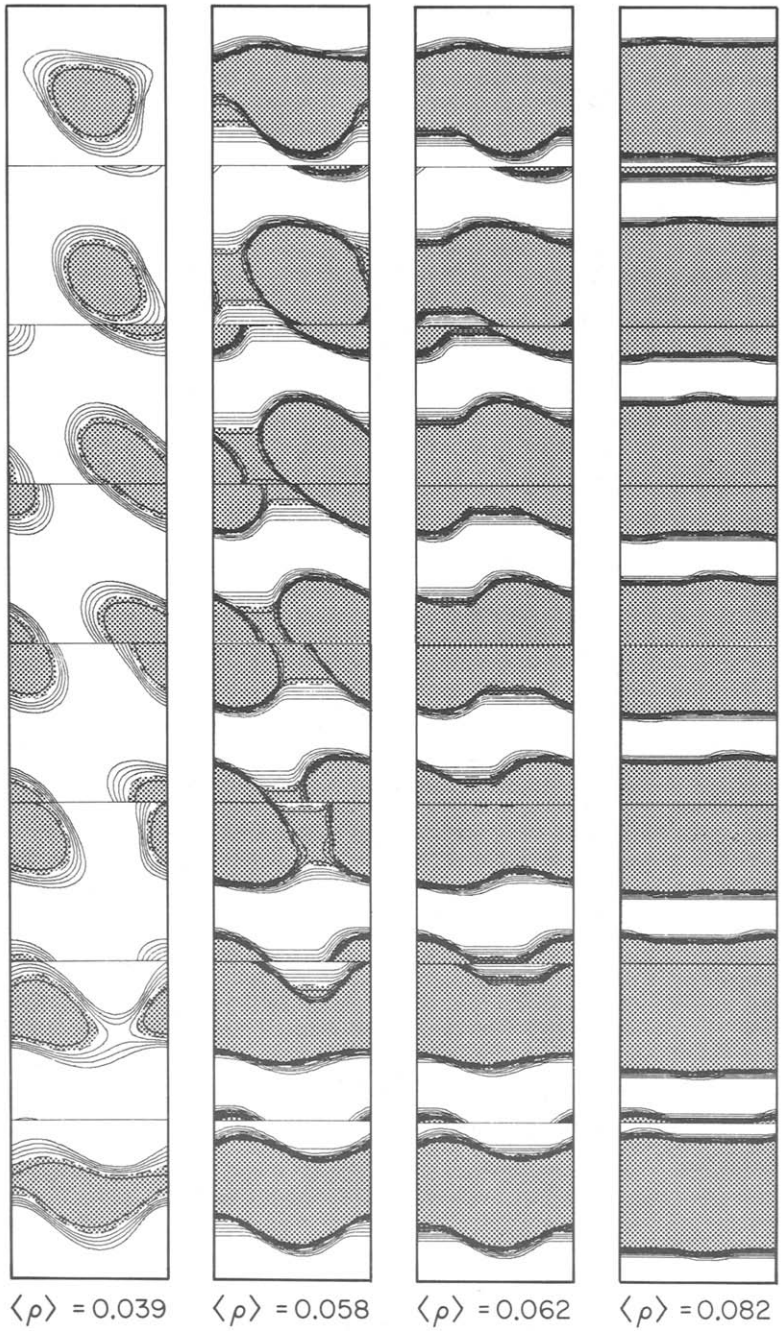

Fig. 5. The nuclear density within the cubic cell for four values of mean density (given in fm^{-3}) corresponding to the adiabatic change from the cross phase to the 1NB phase. Each column is eight contour plots, being equally spaced slices from the unit cell. The cubic unit cell has sides of length L, shown in fig. 2. Note the periodicity of each plot, and also the periodicity from the top to the bottom of each column.

increasing the mean density in small increments. Most of the other data in the figures result from relaxing a well-ordered start derived from the analytic model, with small (10%) random density fluctuations superimposed. These were added so that the system could break symmetries to reduce its energy, but we found that this did not happen. For example, even near the 3N-2N transition, the 3N phase is spherical, not a prolate ellipsoid, and the 2N phase has a circular, not elliptical cross section. Each phase seems to have maximum symmetry whenever it is the thermodynamic phase, although outside this range there are noticeable effects of the artificial cubic symmetry.

4. Conclusions

In this exploratory study, we have shown that nuclear matter below saturation density undergoes several first-order phase transitions, with the pressure discontinuities somewhat greater than has been thought previously. This would tend to disrupt the homologous collapse and weaken the subsequent shock. For densities relevant to stellar collapse ($0.09\ \mathrm{fm}^{-3} \leqslant \langle \rho \rangle \leqslant 0.12\ \mathrm{fm}^{-3}$) the pressure exceeds that of a simple analytical model, by about $0.1\ \mathrm{MeV} \cdot \mathrm{fm}^{-3}$. Although the electron pressure is about $2.8\ \mathrm{MeV} \cdot \mathrm{fm}^{-3}$ at a density of $0.1\ \mathrm{fm}^{-3}$, the formation of a strong shock is so dependent upon the equation of state that this small difference may be important. An increase of pressure acts against gravity to slow the collapse, causing a greater infall of material from the mantle, increasing the radius at which the shock forms, and so weakening the shock.

This work has been an exploratory study of sub-saturation nuclear matter. Possible direct extension would be to study this density regime at finite temperature, with unequal numbers of neutrons and protons, and with different phenomenological forces. The technology we have developed could be applied straightforwardly to such calculations. Another possible extension is the expansion of the variational space to allow separate proton and neutron densities or to improve on the Thomas-Fermi approximation for the kinetic energy density [16]). We have shown that the simple phases (sphere, rod, slab, tube, bubble) are good descriptions of nuclear matter in certain density ranges. It would therefore be interesting to calculate density profiles with one radial coordinate, and variable "dimensionality" [12]) using the Hartree-Fock and Wigner-Seitz approximations.

The major computational effort of our approach is in performing fast Fourier transforms to calculate the Coulomb potential and many relaxation steps are needed because of the disparity between the strengths of the nuclear and Coulomb forces. In addition, the mesh must be fine enough to resolve the nuclear surface for an accurate evaluation of the surface energy. The maximum cell size we used was 32 fm, which certainly cannot be considered large compared to nuclear sizes. Using a 64^3 mesh would help, and indeed is feasible, but the computational effort would be quite large. One approximation worthy of further investigation is to represent

only the location of the nuclear surface, rather than the entire density field, perhaps by a flexible shape parametrization. Inside the shape would be a uniform density, determined by minimization of the internal energy; the volume, surface area, and Coulomb potential can then be expressed as surface integrals [20]).

This work was supported in part by the National Science Foundation, grants PHY82-15500 and PHY82-07332.

References

1) G. Bertsch and D. Mundinger, Phys. Rev. **C17** (1978) 1646
2) G.E. Brown, H.A. Bethe and G. Baym, Nucl. Phys. **A375** (1982) 481
3) H.A. Bethe, J.H. Applegate and G.E. Brown, Ap. J. **241** (1980) 343
4) Supernovae, a survey of current research, ed. M.J. Rees and R.J. Stoneham (Reidel, Dordrecht, Holland, 1982)
5) H.A. Bethe, G.E. Brown, J. Applegate and J.M. Lattimer, Nucl. Phys. **A324** (1979) 487; Proc. Conf. on collapse and numerical relativity, Toulouse, France, ed. M. Signore (Reidel, Dordrecht, Holland, 1983)
6) J.M. Lattimer and T.J. Mazurek, Ap. J. **246** (1981) 955
7) D.Q. Lamb, J.M. Lattimer, C.J. Pethick and D.G. Ravenhall, Nucl. Phys. **A411** (1984) 449; J.M. Lattimer and C.J. Pethick, Ap. J. **223** (1978) 314
8) J.M. Lattimer, Ann. Rev. Nucl. Part. Sci. **31** (1981) 337
9) E. Suraud and D. Vautherin, Proc. Second Workshop on nuclear astrophysics, Ringberg Castle, Tegernsee, Max-Planck-Institute fur Physik und Astrophysik, Munich 1983, to be published
10) P. Bonche and D. Vautherin, Nucl. Phys. **A372** (1981) 496; P. Bonche, S. Levit and D. Vautherin, Saclay Preprint SPhT/83/85, Nucl. Phys. **A427** (1984) 278
11) D.Q. Lamb, J.M. Lattimer, C.J. Pethick and D.G. Ravenhall, University of Illinois preprint ILL-(TH)-84-11 (1984), to be published
12) D.G. Ravenhall, C.J. Pethick and J.R. Wilson, Phys. Rev. Lett. **50** (1983) 2066
13) J.-R. Buchler and Z. Barkat, Phys. Rev. Lett. **27** (1971) 48
14) T.H.R. Skyrme, Nucl. Phys. **9** (1959) 615; D. Vautherin and D.M. Brink, Phys. Lett. **32B** (1970) 149; Phys. Rev. **C5** (1972) 626
15) G. Baym, H.A. Bethe and C.J. Pethick, Nucl. Phys. **A175** (1971) 225
16) B. Grammaticos and A. Voros, Ann. of Phys. **123** (1978) 359
17) S. Levit, Weizmann Institute of Science preprint WIS-84/3/Jan-Ph (1984); K.T.R. Davies, H. Flocard, S. Krieger and M.S. Weiss, Nucl. Phys. **A342** (1980) 111
18) D. Young, Trans. Am. Math. Soc. **76** (1954) 92
19) F. Reif, Fundamentals of statistical and thermal physics (McGraw-Hill, New York, 1965) p. 306
20) K.T.R. Davies and A.J. Sierk, J. Comp. Phys. **18** (1975) 311; K.T.R. Davies and J.R. Nix, Phys. Rev. **C14** (1976) 1977